PROCEEDINGS OF SCIENCE

Diffuse Radio Emission in Galaxy Clusters: Observational Evidence

Reinout J. van Weeren[*†]
Harvard-Smithsonian Center for Astrophysics, 60 Garden Street, Cambridge, MA 02138, USA
E-mail: rvanweeren@cfa.harvard.edu

In a growing number of merging galaxy clusters diffuse extended radio emission has been found, in the form of halos and relics. The existence of this diffuse radio emission implies the presence of relativistic particles and magnetic fields in the intracluster medium. Important questions are how these relativistic particles are accelerated and the role of cluster-wide magnetic fields. Since halos and relics have steep synchrotron spectra they are best studied at low frequencies. Recently, the first deep and high-resolution low-frequency observations of a galaxy cluster have been obtained with LOFAR. An important aspect of this achievement is the development of advanced calibration techniques that allow close to thermal noise limited imaging at frequencies around 150 MHz.

EXTRA-RADSUR2015 (*)
20–23 October 2015
Bologna, Italy

(*) This conference has been organized with the support of the Ministry of Foreign Affairs and International Cooperation, Directorate General for the Country Promotion (Bilateral Grant Agreement ZA14GR02 - Mapping the Universe on the Pathway to SKA)

[*]Speaker.
[†]Clay fellow

PoS(EXTRA-RADSUR2015)038

1. Introduction

In a growing number of merging galaxy clusters diffuse extended radio emission has been found. These sources are usually referred to as radio relics and halos, depending on their location, polarization properties, and morphology (for reviews see Feretti et al., 2012; Brunetti & Jones, 2014). The synchrotron radiation observed with radio telescope indicates the presence of μGauss magnetic fields and relativistic particles (GeV) in the intracluster medium (ICM). The large extent of these sources, in combination with the limited synchrotron lifetime, implies that the relativistic particles (cosmic rays) are(re-)accelerated or produced in-situ (e.g., Jaffe, 1977). The radio spectra of halos and relics are steep, with $\alpha \lesssim -1$ ($F_\nu \propto \nu^\alpha$, where α is the spectral index). Therefore these sources are best studied at relatively low radio frequencies.

Radio halos are centrally located and have typical sizes of about one Mpc. They have smooth brightness distributions, with the radio emission roughly following the X-ray emission from the thermal ICM. For radio halos, there is a correlation between the cluster mass (often the X-ray luminosity or the integrated Compton-y parameter are used as proxies for mass) and radio power (e.g., Cassano et al., 2013; Cassano, 2010). Two main classes of models have been proposed to explain radio halos. In the primary model, electrons are re-accelerated by merger induced magnetohydrodynamical turbulence (e.g., Brunetti et al., 2001; Petrosian, 2001). In the secondary model, the electrons are secondary products of hadronic collision in the ICM (e.g., Dennison, 1980; Blasi & Colafrancesco, 1999; Dolag & Enßlin, 2000; Miniati et al., 2001; Keshet & Loeb, 2010; Enßlin et al., 2011).

Radio relics are polarized elongated sources found in the outskirts of clusters. Most likely, these relics trace shocks where particles are being (re-)accelerated (Enßlin et al., 1998). Evidence that supports this interpretation are the observed high polarization fraction (e.g., Bonafede et al., 2009; van Weeren et al., 2010), the presence of spectral index gradients (e.g., Giacintucci et al., 2008; Kale et al., 2012; Stroe et al., 2013; de Gasperin et al., 2015), and the X-ray surface brightness discontinuities and corresponding temperature changes which indicate the presence of shocks (e.g., Finoguenov et al., 2010; Macario et al., 2011; Ogrean & Brüggen, 2013; Akamatsu & Kawahara, 2013; Shimwell et al., 2015). The precise acceleration mechanism at shocks is still being debated (e.g., Guo et al., 2014; Kang, 2015; Fujita et al., 2015), because in some cases shocks are observed without relics (Russell et al., 2011), and for other relics an unrealistic fraction of the shock energy needs to be transferred to relativistic electrons if these particles are accelerated from the thermal pool (e.g., Vazza & Brüggen, 2014; Pinzke et al., 2013). One potential solution to the above mentioned problems is that the shocks re-accelerate a population of mildly relativistic fossil electrons (e.g., Markevitch et al., 2005; Kang & Ryu, 2011; Kang et al., 2012; van Weeren et al., 2013; Bonafede et al., 2014).

Observations at low frequencies can provide an important contribution to our understudying of diffuse cluster radio sources. For example, the primary model for radio halos predicts a population of ultra-steep spectrum halos that are only visible at low radio frequencies (Brunetti et al., 2008). Low-frequency observations are also best suited to reveal the presence of fossil plasma that could be re-accelerated at shocks. In addition, to produce high-quality spectral index maps a large frequency baseline is required. Low-frequency observations play an important role here by complementing deep maps obtained at frequencies $\nu \gtrsim 1$ GHz.

LOFAR is a new radio telescope operating at frequencies between 10 and 250 MHz (van Haarlem et al., 2013). The 120–180 MHz band (HBA) is best suited for detailed studies of diffuse cluster radio emission because it is the most sensitive part of the observing band. In terms of depth and resolution, LOFAR observations are well matched to observations made with the Karl G. Jansky Very Large Array (JVLA) and Giant Metrewave Radio Telescope (GMRT). In addition, LOFAR has good short baseline coverage to detect diffuse low surface brightness emission from radio halos. One of the main challenges is the calibration and imaging of LOFAR data due the presence of the ionosphere and the complex phased-array station beams. To overcome these challenges a new calibration technique (*facet calibration*) was developed (van Weeren et al., 2016a; Williams et al., 2016). The first application of this new calibration scheme was the 'Toothbrush' (RX J0603.3+4214) galaxy cluster (van Weeren et al., 2016b). This merging cluster is known to host an exceptionally bright radio relic and a extended radio halo (van Weeren et al., 2012; Brüggen et al., 2012; Ogrean et al., 2013; Itahana et al., 2015; Stroe et al., 2016; Jee et al., 2016).

2. Facet calibration

The main challenge for calibrating low-frequency data is the ionosphere (e.g., Lonsdale, 2005; Intema et al., 2009). The ionosphere creates delay differences between antenna stations causing errors in the phases of the measured visibilities. The phase change is related to the differential free electron column density (dTEC). These phase errors are proportional to $\propto \mathrm{dTEC}/\nu^{-1}$, vary across the field of view, and typically change on timescales of 10 sec on a 10^2 km baseline at 150 MHz. In addition to ionospheric phase errors, there are errors from the imperfect knowledge of the time varying stations beams.

The main idea behind the facet calibration scheme is that one can divide up the sky into a few dozen "facets", in which the direction dependent effects are approximately constant. Facet calibration builds upon the "peeling" technique (e.g., Noordam, 2004), where calibration solutions in a discrete number of directions are obtained, similar to other low-frequency calibration schemes (e.g., SPAM, Sagecal, and MeqTrees; Intema et al., 2009; Kazemi et al., 2011; Smirnov, 2011; Noordam & Smirnov, 2010). An example of a sky tessellation is shown in Figure 1.

To reduce the number of parameters in the calibration, only the ionospheric[1] phases are solved for on the shortest timescales. The $\propto \mathrm{dTEC}/\nu^{-1}$ of the phases is directly taken into account, making use of the extra constraints that the wide band data provides. Parallel hand gain solutions are obtained on longer timescales of ~ 10 min, to correct for station beam model errors. The calibration proceeds from facet to facet, slowly building up a picture of the field of view. While computationally intensive, facet calibration produces close to thermal noise limed images, 0.1 mJy beam^{-1} for a typical 8 hr synthesis run, at resolution of $5''$ in the 120–180 MHz HBA band. An example of the improvement obtained at the various stages of facet calibration is shown in Figure 2.

3. Results

We applied the facet calibration scheme to the Toothbrush galaxy cluster for which we also have deep Chandra data available. Figure 3 shows the LOFAR 120–181 MHz high-resolution

[1] Instrumental clock offsets are removed using a calibrator source.

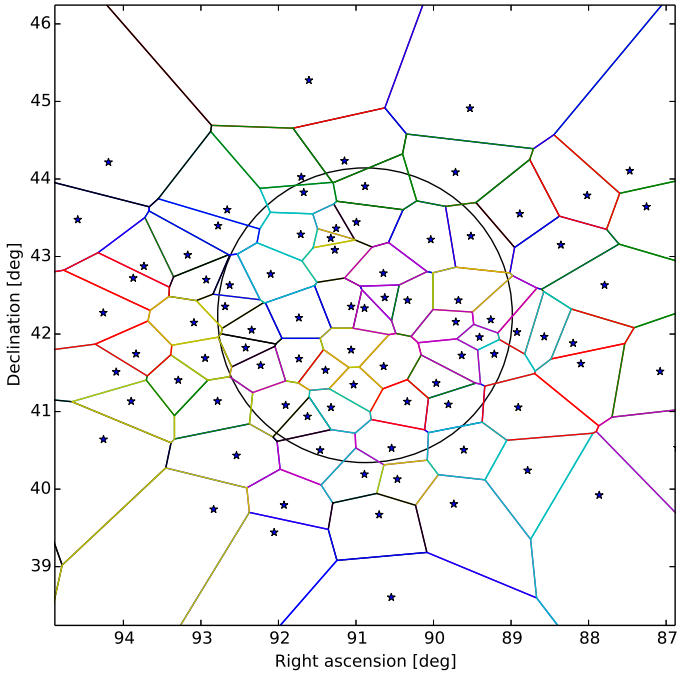

Figure 1: An example of the sky tessellation used for the Toothbrush galaxy cluster field (van Weeren et al., 2016a). The black circle shows the half power beam width and the star symbols represent the centers of the facets.

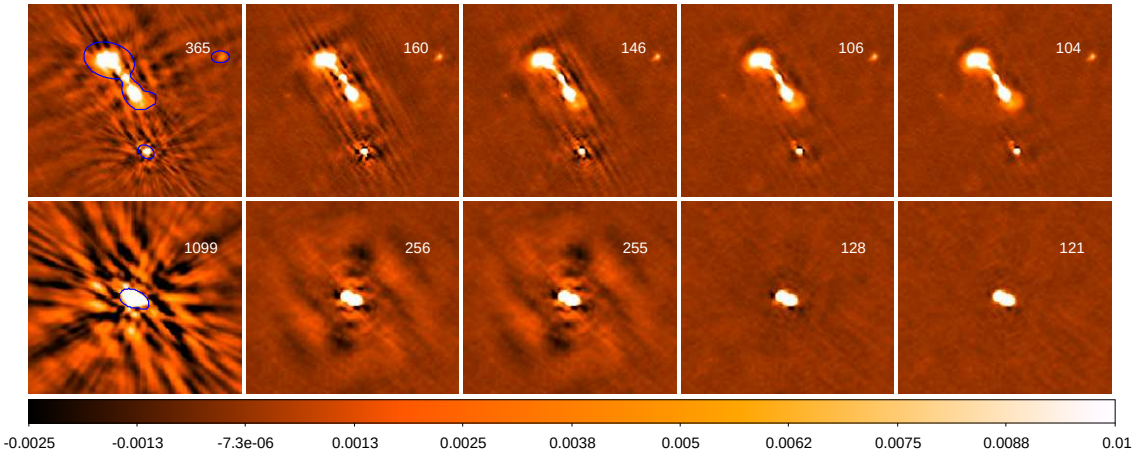

Figure 2: Images showing the improvements at various stages during the direction dependent calibration for two sources, starting with the direction independent self-calibration images on the left side (van Weeren et al., 2016a). The blue contours show the mask used for the deconvolution. The images have a resolution of $8.0'' \times 6.5''$. The scale bar at the bottom is in units of Jy beam^{-1}. The rms noise is indicated in the top right corner in units of μJy beam^{-1}.

($8.0'' \times 6.5''$) image of the cluster compared to a GMRT 150 MHz image with a resolution $26 \times 22''$ (van Weeren et al., 2012). All the known diffuse radio sources in the cluster are clearly detected in the LOFAR image.

We created a spectral index map by combing the data with JVLA 1–2 GHz observations in D-array, see Figure 4. The spectral index map reveals the previously detected (van Weeren et al., 2012) north-south spectral index gradient across the radio relic. We find that the outer edge of the northern Toothbrush relic has a spectral index of $\alpha = -0.8 \pm 0.1$. The spectrum steepens towards the south to $\alpha \approx -2$. The $\alpha = -0.8 \pm 0.1$ correspond to a Mach number of $\mathscr{M} = 2.8^{+0.5}_{-0.3}$, assuming diffusive shock acceleration (DSA). However, our Chandra observations indicate a much weaker shock ($\mathscr{M} \approx 1.2$, with an upper limit of $\mathscr{M} \approx 1.5$) at the relics' outer edge. In addition, computing the kinetic energy flux through the shock surface and comparing that to the observed flux density of the radio relic, we conclude that an unrealistic large fraction of the shocks energy needs to be converted into comic ray electrons. A possible solution to these problems is that of a weak shock re-accelerating old fossil plasma from a radio galaxy. Although, the elongated long linear eastern extent of Toothbrush relic remains puzzling.

The southern edge of the radio halo is well pronounced and coincides with a $\mathscr{M} = 1.39 \pm 0.06$ shock found in the Chandra data. This configuration is very similar to the Bullet Cluster (Markevitch et al., 2002; Shimwell et al., 2014), suggesting a relation between shocks and radio halos. For the radio halo we find an integrated spectral index of $\alpha = -1.08 \pm 0.06$. The spectral index variations across the radio halo are remarkably small, with an intrinsic scatter of $\Delta\alpha \leq 0.04$. This suggest that the turbulence[2] is rather homogeneous on 100 kpc scales in the cluster. Detailed simulations, including the physics of electron acceleration and turbulence, are necessary to draw conclusions on what these finding precisely imply.

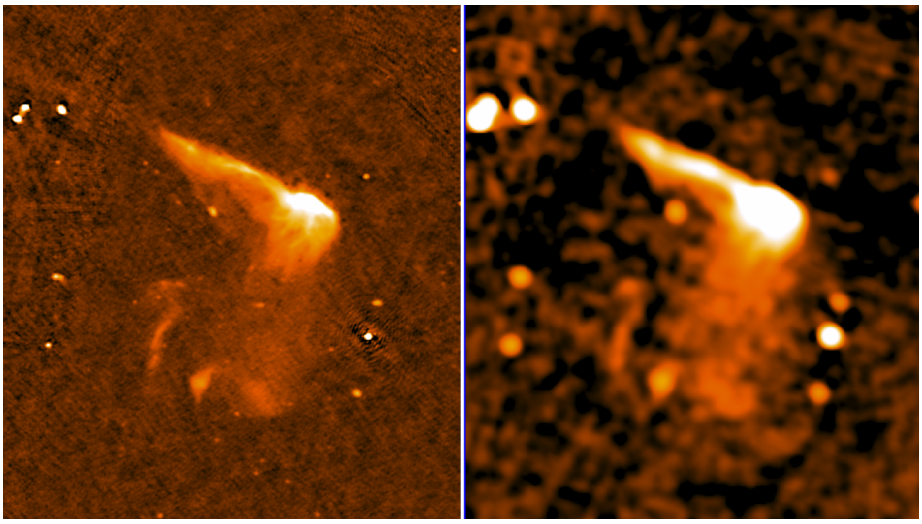

Figure 3: Comparison between a LOFAR HBA and a GMRT 150 MHz image of the Toothbrush galaxy cluster.

[2]assuming the turbulent re-acceleration model is valid

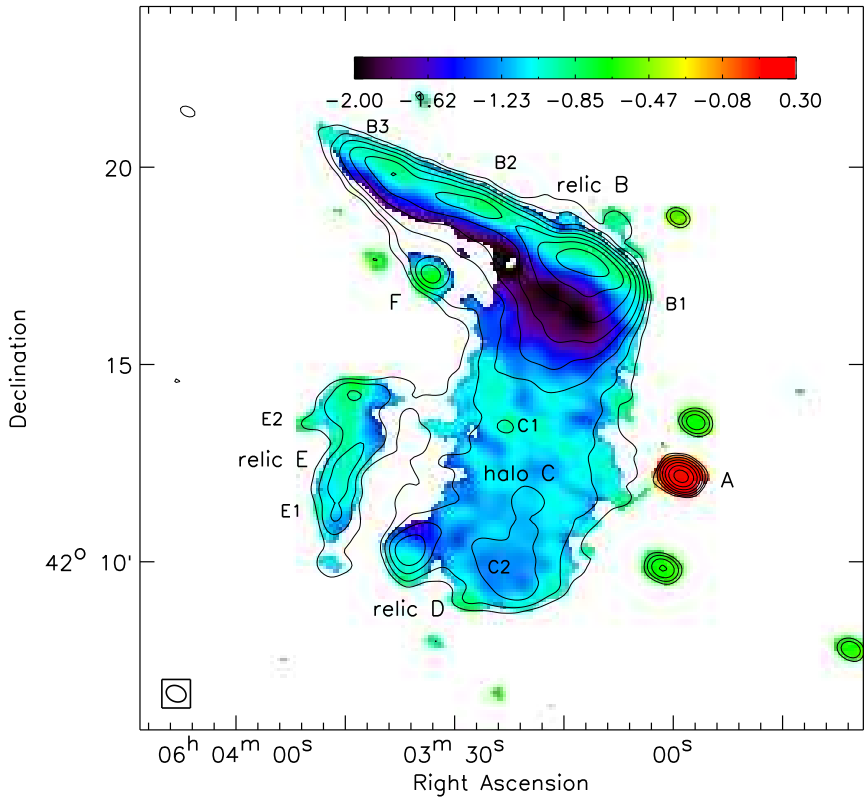

Figure 4: Spectral index map between 0.151 and 1.5 GHz at $31'' \times 24''$ resolution. Sources are labelled as in van Weeren et al. (2012). Contours are drawn at levels of $[1,2,4,\ldots] \times 2$ mJy beam^{-1} and are from the LOFAR image.

4. Summary

We obtained the first deep (0.1 mJy beam^{-1}) high-resolution ($5''$) LOFAR image of a galaxy cluster. This was achieved by employing the facet calibration scheme (van Weeren et al., 2016a) to LOFAR 120–181 MHz observations of the Toothbrush galaxy cluster. The LOFAR data were complemented with 1–2 GHz JVLA observations to create spectral index maps and Chandra observations to characterize the ICM. Our main findings are that the radio properties of the Toothbrush relics seem to be incompatible with DSA and that the spectral index variations across the radio halo are very small ($\Delta\alpha \leq 0.04$). The small spectral index scatter across the halo could imply that the turbulence is rather homogeneous on 100 kpc scales in this cluster.

Acknowledgments

Support for this work was provided by the National Aeronautics and Space Administration through Chandra Award Number GO3-14138X issued by the Chandra X-ray Observatory Center, which is operated by the Smithsonian Astrophysical Observatory for and on behalf of the National Aeronautics Space Administration under contract NAS8-03060. LOFAR, the Low Frequency Array designed and constructed by ASTRON, has facilities in several countries, that are owned by various parties (each with their own funding sources), and that are collectively operated by the International LOFAR Telescope (ILT) foundation under a joint scientific policy. The National Radio Astronomy Observatory is a facility of the National Science Foundation operated under cooperative agreement by Associated Universities, Inc. We

thank the staff of the GMRT that made these observations possible. GMRT is run by the National Centre for Radio Astrophysics of the Tata Institute of Fundamental Research.

References

Akamatsu, H., & Kawahara, H. 2013, PASJ, 65, 16

Blasi, P., & Colafrancesco, S. 1999, Astroparticle Physics, 12, 169

Bonafede, A., Giovannini, G., Feretti, L., Govoni, F., & Murgia, M. 2009, A&A, 494, 429

Bonafede, A., Intema, H. T., Brüggen, M., et al. 2014, ApJ, 785, 1

Brüggen, M., van Weeren, R. J., & Röttgering, H. J. A. 2012, MNRAS, 425, L76

Brunetti, G., & Jones, T. W. 2014, International Journal of Modern Physics D, 23, 30007

Brunetti, G., Setti, G., Feretti, L., & Giovannini, G. 2001, MNRAS, 320, 365

Brunetti, G., Giacintucci, S., Cassano, R., et al. 2008, Nature, 455, 944

Cassano, R. 2010, A&A, 517, A10+

Cassano, R., Ettori, S., Brunetti, G., et al. 2013, ApJ, 777, 141

de Gasperin, F., Intema, H. T., van Weeren, R. J., et al. 2015, MNRAS, 453, 3483

Dennison, B. 1980, ApJ, 239, L93

Dolag, K., & Enßlin, T. A. 2000, A&A, 362, 151

Enßlin, T., Pfrommer, C., Miniati, F., & Subramanian, K. 2011, A&A, 527, A99+

Enßlin, T. A., Biermann, P. L., Klein, U., & Kohle, S. 1998, A&A, 332, 395

Feretti, L., Giovannini, G., Govoni, F., & Murgia, M. 2012, A&A Rev., 20, 54

Finoguenov, A., Sarazin, C. L., Nakazawa, K., Wik, D. R., & Clarke, T. E. 2010, ApJ, 715, 1143

Fujita, Y., Takizawa, M., Yamazaki, R., Akamatsu, H., & Ohno, H. 2015, ApJ, 815, 116

Giacintucci, S., Venturi, T., Macario, G., et al. 2008, A&A, 486, 347

Guo, X., Sironi, L., & Narayan, R. 2014, ApJ, 797, 47

Intema, H. T., van der Tol, S., Cotton, W. D., et al. 2009, A&A, 501, 1185

Itahana, M., Takizawa, M., Akamatsu, H., et al. 2015, PASJ, 67, 113

Jaffe, W. J. 1977, ApJ, 212, 1

Jee, M. J., Dawson, W. A., Stroe, A., et al. 2016, ApJ, 817, 179

Kale, R., Dwarakanath, K. S., Bagchi, J., & Paul, S. 2012, MNRAS, 426, 1204

Kang, H. 2015, Journal of Korean Astronomical Society, 48, 155

Kang, H., & Ryu, D. 2011, ApJ, 734, 18

Kang, H., Ryu, D., & Jones, T. W. 2012, ApJ, 756, 97

Kazemi, S., Yatawatta, S., Zaroubi, S., et al. 2011, MNRAS, 414, 1656

Keshet, U., & Loeb, A. 2010, ApJ, 722, 737

Lonsdale, C. J. 2005, in Astronomical Society of the Pacific Conference Series, Vol. 345, From Clark Lake to the Long Wavelength Array: Bill Erickson's Radio Science, ed. N. Kassim, M. Perez, W. Junor, & P. Henning, 399

Macario, G., Markevitch, M., Giacintucci, S., et al. 2011, ApJ, 728, 82

Markevitch, M., Gonzalez, A. H., David, L., et al. 2002, ApJ, 567, L27

Markevitch, M., Govoni, F., Brunetti, G., & Jerius, D. 2005, ApJ, 627, 733

Miniati, F., Jones, T. W., Kang, H., & Ryu, D. 2001, ApJ, 562, 233

Noordam, J. E. 2004, in Society of Photo-Optical Instrumentation Engineers (SPIE) Conference Series, Vol. 5489, Society of Photo-Optical Instrumentation Engineers (SPIE) Conference Series, ed. J. M. Oschmann, Jr., 817–825

Noordam, J. E., & Smirnov, O. M. 2010, A&A, 524, A61

Ogrean, G. A., & Brüggen, M. 2013, MNRAS, 433, 1701

Ogrean, G. A., Brüggen, M., van Weeren, R. J., et al. 2013, MNRAS, 433, 812

Petrosian, V. 2001, ApJ, 557, 560

Pinzke, A., Oh, S. P., & Pfrommer, C. 2013, MNRAS, 435, 1061

Russell, H. R., van Weeren, R. J., Edge, A. C., et al. 2011, MNRAS, 417, L1

Shimwell, T. W., Brown, S., Feain, I. J., et al. 2014, MNRAS, 440, 2901

Shimwell, T. W., Markevitch, M., Brown, S., et al. 2015, MNRAS, 449, 1486

Smirnov, O. M. 2011, A&A, 527, A107

Stroe, A., van Weeren, R. J., Intema, H. T., et al. 2013, A&A, 555, A110

Stroe, A., Shimwell, T., Rumsey, C., et al. 2016, MNRAS, 455, 2402

van Haarlem, M. P., Wise, M. W., Gunst, A. W., et al. 2013, A&A, 556, A2

van Weeren, R. J., Röttgering, H. J. A., Brüggen, M., & Hoeft, M. 2010, Science, 330, 347

van Weeren, R. J., Röttgering, H. J. A., Intema, H. T., et al. 2012, A&A, 546, A124

van Weeren, R. J., Fogarty, K., Jones, C., et al. 2013, ApJ, 769, 101

van Weeren, R. J., Williams, W. L., Hardcastle, M. J., et al. 2016a, ArXiv e-prints 1601.05422

van Weeren, R. J., Brunetti, G., Brüggen, M., et al. 2016b, ArXiv e-prints 601.06029

Vazza, F., & Brüggen, M. 2014, MNRAS, 437, 2291

Williams, W. L., van Weeren, R. J., Röttgering, H. J. A., Best, P., & et al. 2016, MNRAS, submitted